# Quantum phase transition in the Frenkel-Kontorova chain: From pinned instanton glass to sliding phonon gas

O. V. Zhirov*
*Budker Institute of Nuclear Physics, 630090 Novosibirsk, Russia*

G. Casati†
*International Center for the Study of Dynamical Systems, Università degli Studi dell'Insubria, Como, Italy; Istituto Nazionale per la Fisica della Materia, Unità di Como, Via Valleggio 11, 22100 Como, Italy; and Istituto Nazionale di Fisica Nucleare, Sezione di Milano, Via Celoria 16, 20133 Milano, Italy*

D. L. Shepelyansky‡
*Laboratoire de Physique Quantique, UMR 5626 du CNRS, Université Paul Sabatier, 31062 Toulouse, France*
(Received 17 October 2002; published 19 May 2003)

We study analytically and numerically the one-dimensional quantum Frenkel-Kontorova chain in the regime where the classical model is located in the pinned phase characterized by the gaped phonon excitations and devil's staircase. By extensive quantum Monte Carlo simulations, we show that for the effective Planck constant $\hbar$ smaller than the critical value $\hbar_c$ the quantum chain is in the pinned instanton glass phase. In this phase, the elementary excitations have two branches: *phonons*, separated from zero energy by a finite gap, and *instantons* that have an exponentially small excitation energy. At $\hbar=\hbar_c$ the quantum phase transition takes place and for $\hbar>\hbar_c$ the pinned instanton glass is transformed into the sliding phonon gas with gapless phonon excitations. This transition is accompanied by the divergence of the spatial correlation length and appearance of sliding modes at $\hbar>\hbar_c$.

DOI: 10.1103/PhysRevE.67.056209 PACS number(s): 05.45.−a, 63.70.+h, 61.44.Fw

## I. INTRODUCTION

The Frenkel-Kontorova (FK) model [1] describes a one-dimensional chain of atoms or particles with harmonic couplings placed in a periodic potential. This model was introduced more than sixty years ago with the aim to study crystal dislocations [1,2]. It was also successfully applied later to the description of commensurate-incommensurate phase transitions [3], epitaxial monolayers on the crystal surface [4], ionic conductors and glassy materials [5–7], and, more recently, to charge-density waves [8] and dry friction [9,10]. Despite the fact that the relevant phenomena are at the atomic scale, all these works are based essentially on the classical approach. The first study of quantum effects was done twelve years ago [11–13] with the attempt to understand the highly nontrivial quantum ground state of the Frenkel-Kontorova model in the regime where the classical ground state is characterized by the fractal ''devil's staircase'' [6]. These studies were extended in Refs. [14,15] and later the quantum dynamics at different values of quantum parameter $\hbar$ was studied in Refs. [16–20].

The physical properties even of the classical FK model are very rich and nontrivial. In 1978 Aubry discovered [6] a new type of ground state that has fractal properties known as ''devil's staircase.'' In fact, the equilibrium positions of atoms in the FK chain are described [6] by the well known Chirikov standard map [21], which describes generic properties of chaotic Hamiltonian dynamics. The density of particles in the equilibrium state determines the rotation number of the invariant curves of the map, while the amplitude of the periodic potential in the FK model gives the value of the dimensionless parameter $K$. According to the known properties of the map, it follows that there exist two phases of the chain, the ''sliding'' phase and the ''pinned'' phase. Indeed at $K<K_c$ the Kolmogorov-Arnold-Moser (KAM) curves are smooth and the chain can easily slide along the potential. This implies the existence of a zero phonon mode. In contrast, at $K>K_c$ the KAM curves are destroyed and replaced by an invariant cantor set that is called cantorus [6,22–25]. In this pinned phase the chain cannot slide being kept by a finite Peierls-Nabarro barrier and the phonon spectrum is separated from zero by a finite gap. In this paper, we consider only the gaped-pinned phase with $K>K_c$.

It is important to stress that in the pinned phase, besides the equilibrium state of minimal energy, there exists a lot of other *equilibrium* configurations, corresponding to *local* minima of the potential with energies very close to the minimal energy, i.e., the energy of the ground state [26–28]. The total amount of these states (configurational excitations) grows exponentially both with the length $L$ of the chain, as well as with the parameter $K$ [28]. Moreover, a great number of them is practically degenerate since their energy separation from the ground state is exponentially small.

In the classical limit all these configurational excitations are stable, while in the quantum case they become metastable due to tunneling between different exponentially degenerate minima of the potential. As a result one may expect that the true eigenstates of the Hamiltonian, including the ground state, are built as superpositions of classical configu-

*Electronic address: zhirov@inp.nsk.su
†Electronic address: giulio.casati@uninsubria.it
‡Electronic address: dima@irsamc.ups-tlse.fr

 

rational states. Such a nontrivial structure of the quantum ground state of the chain has a profound analogy with the famous vacuum of quantum chromodynamics (QCD) [29], in which tunneling transitions between different, practically degenerate, states are known as ''instantons.'' This analogy between the two problems is very useful and implies that many of the methods developed in lattice QCD studies may be applicable to the quantum FK model.

Dynamical low-energy excitations in the classical FK chain consist only of phonon modes describing small vibrations around a classical minimum of the chain potential energy. In the quasiclassical regime, where the effective dimensionless Planck constant $\hbar$ is very small, the quantization of the FK chain can be reduced to a quantization of phonon modes only. Indeed the time of tunneling between different minima of the potential energy is exponentially large, compared to periods of the vibrations, and the phonon modes are decoupled from the tunneling modes (instantons). This reminds the situation in the QCD [29] where the quasiclassical regime for instantons appears at small distances on which instantons are also decoupled from other excitations such as quarks and gluons.

In this regime, the tunneling transitions are very slow, instantons are local and frozen in space. Due to exponential degeneracy of chain configurations the model reveals a glasslike structure of instantons randomly distributed along the chain. We will call this phase the ''instanton glass.''

One may expect that the phase structure changes significantly with the increase of $\hbar$ when the tunneling time $t \sim \exp(S_{in}/\hbar)$ ($S_{in}$ is the instanton action) becomes comparable to the inverse frequency of phonons. In this case, phonon and instanton excitations can strongly influence each other due to anharmonicity of the periodical potential. This may lead to quantum melting of the instanton glass phase and transition to another phase which appears above some critical value $\hbar > \hbar_c$.

The existence of another quantum phase can be argued in the following way. At sufficiently large $\hbar \geqslant \hbar_c$ the kinetic energy of quantum particle $E_k \sim \hbar^2/2m(\Delta x)^2$ starts to exceed the height $U$ of the periodic potential in which the chain is placed (here $\Delta x$ is the mean particle separation in the chain which is comparable with the period of the potential, $m$ is the particle mass). The condition $E_k \sim U$ gives $\hbar_c \sim \Delta x\sqrt{mU}$. As a result, for $\hbar > \hbar_c$ the chain turns from the *pinned* to the *sliding* phase. In this regime, tunneling is replaced by direct propagation above the barrier. Hence, the instantonlike motion is replaced by phononlike motion corresponding to a new phase with gapless phonon excitations. This regime can be considered as sliding quantum phase similar to classical sliding regime at $K < K_c$ [23,24]. Qualitative different types of behavior of the quantum FK model at small and large $\hbar$ values were already seen in the first numerical studies [11,12]. In summary, at $\hbar = \hbar_c$ one may expect a *quantum phase transition*, with qualitative rearrangement of the spectrum of elementary quasiparticle excitations.

In this work, devoted to a comprehensive numerical study of the transition we have just outlined, we present a complete picture of low-energy excitations in the quantum FK chain. We also find that this transition is highly nontrivial and the model reveals a nonanalytical behavior that can partially explain the failure of simple analytical approaches developed in Refs. [14,16,17,20]. It should be stressed also that our results have relevance to a wider class of quantum systems, e.g., quantum spin glass or other disordered systems with interactions. Indeed, the existence of highly degenerate classically stable configurations is a general property of such systems.

The paper is organized as follows. In Sec. II, we outline the model, its quantum features and the main points of our numerical approach. In Sec. III, we study elementary excitations of the chain at different values of $\hbar$ and show that there exists a structural rearrangement of the excitation spectrum at certain $\hbar = \hbar_c$. A detailed analysis of this rearrangement, given in Sec. IV, indicates that we have a quantum phase transition. Our results are summarized in Sec. V.

## II. THE QUANTUM FRENKEL-KONTOROVA MODEL

### A. Definitions and outline of quantum features

The model describes a one-dimensional chain of particles with harmonic couplings placed in a periodic potential. The Hamiltonian reads

$$H = \sum_{i=0}^{s} \left[ \frac{P_i^2}{2m} + \alpha \frac{(x_i - x_{i-1})^2}{2} - \beta \cos(x_i/d) \right], \qquad (1)$$

where $s$ is the number of particles, $P_i$ and $x_i$ are their momenta and coordinates, and in the quantum case $P_i = -i\hbar\partial/\partial x_i$. In this paper, we use units $m = d = \alpha = 1$ that correspond to dimensionless Hamiltonian (see for details, e.g., Refs. [11,12,14])

$$H = \sum_{i=0}^{s} \left[ \frac{P_i^2}{2} + \frac{(x_i - x_{i-1})^2}{2} - K \cos(x_i) \right], \qquad (2)$$

with a dimensionless parameter $K = \beta/\alpha d^2$ and the dimensionless Planck constant $\hbar$ is measured in units of $d^2\sqrt{m\alpha}$. In this way, $K$ is the chaos parameter in the Chirikov standard map [21,23]. We use the standard boundary conditions

$$x_0 = 0, \quad x_s = L, \qquad (3)$$

where the chain length $L = 2\pi r$ consists of $r$ periods (and wells) of the external field. We analyze the standard case of golden mean ratio corresponding to $r/s \to (\sqrt{5}-1)/2$ (see, Refs. [11,12,28]). The potential energy of the chain,

$$U(\{x\}) = \sum_{i=0}^{s} \left[ \frac{(x_i - x_{i-1})^2}{2} - K \cos(x_i) \right], \qquad (4)$$

has a large number of minima, corresponding to different possible distributions of particles among the wells. The classical ground state (absolute minimum of the potential energy) is characterized by some special ordering discovered by Aubry [6,23,24]. In addition, there are also local minima, known as ''configurational excitation'' states [30]. Many of them have exponentially small energy separations from the

energy of the classical ground state [28]. In the classical case, all these states are well defined (distinguishable) and absolutely stable.

In contrast, in the *quantum* world these states are *metastable* due to quantum tunneling. Since they are practically degenerate with the classical ground state, the actual *quantum* ground state is built by *many* of them. The admixture of metastable classical configurations in the quantum ground state was first discussed in Refs. [14,15]. Let us summarize below the most important aspects of the quantum ground state, related to the tunneling between these configurations.

In the quasiclassical region, the transition amplitudes between different metastable configurations are exponentially small. Hence, the ground state wave function is (with exponential accuracy) a sum of nonoverlapping parts, each referring to a particular classical configuration. Any average over the quantum ground state is (within the same accuracy) a weighted sum of averages over relevant classical configurations. Note that in this limit, the main contribution to quantum motion comes from phonons that characterize small vibrations around a classical equilibrium configuration. In fact, the phonon spectrum is only weakly sensitive to the choice of specific configuration [31] and the influence of tunneling processes on the global (thermodynamical) properties of the chain is expected to be small. In particular, the phonon spectrum is still characterized by a phonon gap similar to the classical case. In this regime, the tunneling transitions between metastable configurations are very slow compared to phonon frequencies and can be considered as well separated instantons.

At higher values of $\hbar$ the tunneling rate increases and becomes comparable with the frequency of phonons. In this regime, phonon oscillations are large and essentially anharmonic and therefore the known analytical approaches [14,16,19,20] based on the gausslike wave-function profile are not quite adequate. Instead, interactions between instantons and phonons come into play here. As it will be shown later, this leads to a new sliding phase appearing at $\hbar > \hbar_c$.

In fact, the effects of quantum tunneling between classical configurations were already seen in the numerical studies [12] [see Fig. 4(b)]. However, they were not attentively analyzed and the mixture of classical metastable configurations induced by quantum tunneling was not discussed. Certainly, tunneling processes affect significantly the average positions of particles at large time scales. Therefore, the quantities based on mean expectation values of particle positions are not adequate even in the deep quasiclassical regime. Hence, the basic concepts of classical treatment, such as hull [6,23] and $g$ functions [11,12], are also not adequate in this quantum regime. The point is that in the case of particle tunneling between two classical equilibrium positions the expectation value does not correspond to any *probable* (in the classical sense) particle position. This is evident from the analogy with the two-well potential problem, where the mean expectation value of a particle position coincides with the *top* of the barrier.

### B. Path integral and numerical simulations

Tunneling effects are best understood in the Feynman path integral formulation of quantum mechanics [32]. In particular, the transformation to "Euclidean" time variable $\tau$; $t = i\tau$ makes the tunneling transition, or *instanton*, local in time $\tau$. In the quasiclassical regime, the tunneling probability is very small and therefore the mean separation between instantons is large compared to their size. This allows to use the approximation of dilute instanton gas [32].

Feynman path formulation in the Euclidean time allows direct numerical simulations of quantum systems with probabilistic treatment [33] of the path integral

$$Z = \int Dx[\tau] \exp\left( -\frac{1}{\hbar} S[x(\tau)] \right), \tag{5}$$

where the Euclidean action,

$$S[x(\tau)] = \int_0^{\tau_0} d\tau \sum_i \left( \frac{\dot{x}_i^2}{2} + \frac{(x_i - x_{i-1})^2}{2} - K\cos(x_i) \right), \tag{6}$$

has the same form as a total energy of a chain of particles in the usual real time variable, integrated over some time interval $[0, \tau_0]$. This is equivalent to the consideration of the quantum system at some finite temperature [33]

$$T = \hbar / \tau_0 . \tag{7}$$

We assume periodic boundary conditions in the *time* direction, which correspond to a path closed on a torus

$$x_i(\tau_0) = x_i(0), \quad i = 1, \ldots, s-1, \tag{8}$$

and integrate over the initial conditions $x_i(0)$ in order to restore homogeneity of paths along the time torus. This allows to improve the statistics in data measurements by averaging the data along the torus.

The numerical simulation of the path integral (5) needs discretization of the time variable $\tau_n = \Delta\tau n$, $n = 1, \ldots, N$ by splitting the time interval $\tau_0$ into $N$ steps of size $\Delta\tau = \tau_0 / N$. As a result the original time-continuous model (2) turns into a two-dimensional lattice model with the action

$$S = \sum_{n=0}^{N} \sum_{i=1}^{s} \left[ \frac{(x_{i,n+1} - x_{i,n})^2}{2\Delta\tau} + \Delta\tau \frac{(x_{i+1,n} - x_{i,n})^2}{2} - \Delta\tau K \cos x_{i,n} \right]. \tag{9}$$

The time step $\Delta\tau$ should be chosen small enough to approach the continuous limit of the original model (2). This leads to the following requirements. At any time step $\Delta\tau$ the path variable $x_i$ jumps by a random shift $\Delta x_i \sim \sqrt{\hbar \Delta\tau}$. The first obvious requirement is that the shift $\Delta x_i$ should be small compared to the spatial scale of the potential energy variation. Another requirement comes from the standard derivation of the path integral [33,34], the potential energy terms should be small compared to the kinetic energy,

$$\Delta\tau \left( \frac{(x_{i+1,n} - x_{i,n})^2}{2} - K\cos x_{i,n} \right) \ll \frac{(x_{i,n+1} - x_{i,n})^2}{2\Delta\tau}. \tag{10}$$

The latter condition makes our lattice *anisotropic* with respect to spatial-time directions. In spite of the common belief [35] on the equivalence between quantum one-dimensional chains and classical two-dimensional statistical (e.g., $XY$) models, the above discussion shows that some particular care has to be taken.

An accurate treatment of particle tunneling between two wells in the chain requires some modifications of action (9). For a finite (not very small) time step $\Delta\tau$, there exists a probability for a particle to jump over the potential barrier in *one* time step [34]. The corresponding path contribution to the action will be strongly underestimated by Eq. (9) and, respectively, the probability of tunneling will be too high. To cure this problem, we use in our simulation an improved [34] version of action (9), with the potential energy term $\Delta\tau U(x_n)$ replaced by the integral $\Delta\tau\int_{x_n}^{x_{n+1}}U(x)dx/(x_{n+1}-x_n)$ along a straight line that links subsequent (in time) points $(x_n,x_{n+1})$ of the particle path. This significantly improves the accuracy of numerical simulations.

For simulations of path ensembles, we use the standard Metropolis algorithm [36]. Each iteration looks as follows: at any fixed time slice at number $n$, we update sequentially the particles coordinates $x_{i,n}$, $i=1,\ldots,s$; then we go to the next time slice $n\to n+1$; and so on.

The system has two principal characteristic relaxation time scales that are originated by different underlying processes. Basically one can estimate the number of iterations as $N_{it}\sim 1/\omega^{(min)}\Delta\tau$, where $\omega^{(min)}$ is the lowest frequency relevant to the process and $\Delta\tau$ is time discretization step. The shortest scale is related to the path relaxation with respect to main phonon modes, and is typically of the order of a few tens of iterations in the quasiclassical regime, where phonons have a gap of the order of unity. Another time scale is much larger and is determined by the smallest frequency related to either the tunneling rate between different classical configurations, or to the lowest phonon frequency available in the system for $\hbar\geqslant\hbar_c$.

For the initial state, we choose the Aubry classical ground state. Then, applying iterations, we generate a path ensemble. To be sure that the system does actually relax to statistical equilibrium with respect to the slowest processes described above, we control the mean number of particle path crossings over tops of potential barriers and we discard all configurations in the ensemble until this quantity stabilizes. All computations are done for the chaos parameter $K=5$. The required number of iterations to reach relaxation is very sensitive to the value of quantum parameter $\hbar$: for example, at $\hbar=3$ this number is $N_{it}\sim(2-4)\times10^2$, while at $\hbar=1$ it is of the order of $10^5$–$10^6$. This explains why in the first studies [11,12] done at $N_{it}\leqslant10^4$ many details at $\hbar\leqslant2$ were not seen. We study chains with up to 233 particles.

## III. ELEMENTARY EXCITATIONS

The most important information about the quantum system is contained in its spectrum of low-lying elementary excitations. Being the net manifestation of system internal structure it reflects any structural transition that can occur in the system, and it provides a complete description of low-temperature thermodynamic and kinetic properties. We extract this spectrum using an approach based on the analysis of Fourier spectrum of Feynman paths. This approach provides a most direct way to see and resolve different excitations in the system. Then, we compare our method with the more traditional one, based on the study of time correlation functions. This comparison provides a self-consistency check and demonstrates the advantages of our method.

### A. Spectral properties of Feynman paths

In classical nonlinear dynamics, the Fourier analysis of trajectories plays a key role in understanding of periodic motion of complex systems. In a similar way, the spectral characteristics of Feynman paths are closely related to the properties of elementary excitations in quantum systems. We start our studies from the quasiclassical limit $\hbar\to0$, where this relation is exact, and extend them to higher values of $\hbar$.

Let us consider the Fourier image of the path variable $x_i(\tau)$;

$$a_i(\omega_m)=\frac{1}{\sqrt{\tau_0}}\int_0^{\tau_0}d\tau\, x_i(\tau)\exp(i\omega_m\tau), \tag{11}$$

where $\omega_m=m\varpi$, $\varpi\equiv2\pi/\tau_0$, and $-\infty<m<\infty$. The path variable $x_i(\tau)$ is real, therefore $a_i(-\omega_m)=[a_i(\omega_m)]^*$. To get insight into the physical content of this quantity let us consider the quasiclassical regime $\hbar\ll1$. Then, for small variations $x_i(\tau)=\overline{x_i}+\delta x_i(\tau)$ around the classical static trajectory $\{\overline{x_i}\}$, one can expand action (6) up to the second-order terms in $\delta x_i(\tau)$. Next, using the spectral expansion for $\delta x_i(\tau)$ and performing the integration over $\tau$, one gets

$$S=S_0[\overline{x}]+\sum_m\sum_{i,k}\frac{1}{2}(\omega_m^2\delta_{ik}-\Omega_{ik}^2)a_i(-\omega_m)a_k(\omega_m), \tag{12}$$

$$\Omega_{ik}^2=\delta_{ik}(2+K\cos(x_i))-\delta_{i,k-1}-\delta_{i-1,k}. \tag{13}$$

Now, by the transformation to normal modes $A^{(l)}(\omega_m)=\Sigma_i V_i^{(l)}a_i(\omega_m)$, where eigenvectors $V_i^{(l)}$ satisfy the equation $\Omega_{ik}^2V_k^{(l)}=\nu_l^2V_i^{(l)}$, one gets the standard representation of the action as a sum of independent phonon modes:

$$S=S_0[\overline{x}]+\sum_m\sum_l\frac{1}{2}(\omega_m^2+\nu_l^2)|A^{(l)}(\omega_m)|^2. \tag{14}$$

Finally, the path integral (5) turns into a product of ordinary integrals

$$Z=\int\prod_{l=1}^{s-1}dA^{(l)}(0)\exp[-\nu_l^2|A^{(l)}(0)|^2/2\hbar]$$
$$\times\prod_{m=1}^{\infty}d\,\mathrm{Re}\,A^{(l)}(\omega_m)d\,\mathrm{Im}\,A^{(l)}(\omega_m)$$
$$\times\exp[-(\omega_m^2+\nu_l^2)|A^{(l)}(\omega_m)|^2/\hbar],$$

and one arrives to the well known result for the correlator of free phonon modes:

$$\langle A^{(l)}(\omega_m)A^{(l)*}(\omega_{m'})\rangle = \frac{\hbar\,\delta_{mm'}}{(\omega_m^2+\nu_l^2)}. \tag{15}$$

We note that this result is obtained from Eq. (6), where the action is *continuous* in time variable. In the discretized version (9), the number of harmonics is finite: $|m| = 0,1,\ldots,M$, where $M=\tau_0/2\Delta\tau$. It can be shown that the only modification induced by discretization is the replacement in Eq. (15): $\omega_m \to \tilde{\omega}_m = (2\omega_M/\pi)\sin(\pi\omega_m/2\omega_M)$, $\omega_M \equiv M\varpi$. As a result, the spectral function for phonons is given by

$$F^{(l)}(\tilde{\omega}_m) \equiv \langle |A^{(l)}(\omega_m)|^2\rangle = \frac{\hbar}{(\tilde{\omega}_m^2+\nu_l^2)}. \tag{16}$$

Hereafter, instead of $\omega_m$ we assume its discretized version $\tilde{\omega}_m$, and in the following the tilde will be omitted.

The expression (15) is the well known Wick rotated Green function (in the frequency representation) for a single free particle in the phonon field theory, which has in our case one spatial dimension.

In the quasiclassical regime, the amplitudes of phonon oscillations are small and the interactions between phonons due to anharmonicity of Hamiltonian (2) are negligible. At higher $\hbar$, the amplitudes of phonon vibrations grow as $\hbar^{1/2}$ and their interactions become more important. In general, interactions can essentially modify the Green function (15) for phonon excitations. This actually happens for $\hbar > \hbar_c$, where the spectrum of excitations is significantly changed. However, one may expect that the spectral function of elementary excitation remains of the same form

$$F^{(l)}(\omega_m) = f\frac{\hbar}{(\omega_m^2+\nu_l^2)}, \tag{17}$$

which differs from Eq. (15) by the renormalized frequency value $\nu_l$ and by an overall renormalization factor $f$, in analogy with the Green function behavior in the renormalizable quantum field theories (see, e.g., Ref. [29]). In fact, this idea is well supported by numerical data.

An extended elementary excitation involves all particles in the chain. In turn, the Fourier harmonics of any particle coordinate in the chain are a sum of contributions of many elementary excitations

$$\langle |a_i(\omega_m)|^2\rangle = \sum_j f_i^{(j)}\frac{\hbar}{(\omega_m^2+\nu_j^2)}, \tag{18}$$

where the sum goes over all chain excitations. In the deep quasiclassical case, the main contribution comes from phonons modes, and the sum goes over phonon modes $l$, with $f_i^j \to |V_i^{(l)}|^2$ and $\nu_j \to \nu_l$.

The goal of our study here is a complete picture of low-lying quantum excitations in the chain, both for low and high values of $\hbar$. In fact, the spectrum of low-lying excitations is crucially dependent on $\hbar$; there are domains with a *qualitatively* different behavior. In order to illustrate this, let us consider the amplitude of quantum motion of particles in the chain, given by Eq. (18). It is seen that the contributions of low-frequency modes (small $\nu_l$) dominate in the limit $\omega_m \to 0$, provided that their wave-function profiles $V_i^{(l)}$ are not small at the particle position $i$. Therefore, the spectral function (18), computed in this limit, gives a rough estimate for the frequency $\nu_l$ of the lowest mode.

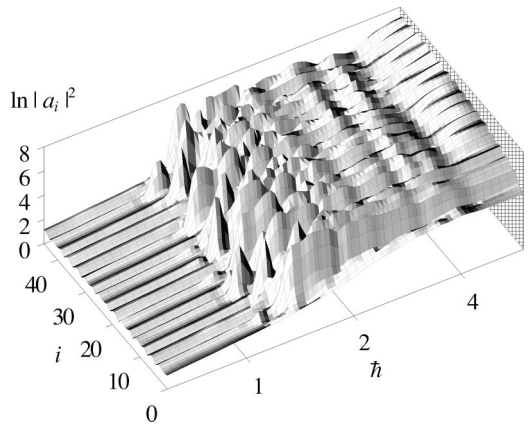


FIG. 1. Dependence of the amplitude of the lowest Fourier harmonic $a_i \equiv a_i(\omega_1)$ on the particle position $i$ in the chain at different $\hbar$. Here, $\omega_1 = \varpi = 2\pi/\tau_0$, $m=1$. The chain parameters are $s/r = 89/55$, $K=5$, and $\tau_0 = 80$. Typical number of iterations is $(1.5\text{–}5)\times 10^5$ at each value of $\hbar$. Here and in all other figures the units are dimensionless (see text for the definition of model parameters).

In Fig. 1, the amplitude of the *lowest* Fourier harmonic $a_i(\omega_1)$ with $\omega_1 = \varpi = 2\pi/\tau_0$ is plotted as a function of the particle position $i$ at different $\hbar = 0.6-8$. One can see that the whole interval of $\hbar$ splits naturally in *three* regions of qualitatively different behavior: (i) the quasiclassical region $\hbar \lesssim 1$, where the amplitudes $a_i(\omega_1)$ of the harmonics are very small and depend on the particle positions in some regular way; (ii) the transition region $1 \lesssim \hbar \lesssim 2$, where this dependence is highly irregular and interactions between instantons and phonons are important; and (iii) the region $\hbar \gtrsim 2$, where this dependence becomes regular again and where, as we shall see below, a new phonon branch appears. Let us note, that at $\hbar < 1$ the regular structure along the chain is quasiperiodical, which reflect a fact that a classical chain is built of ''bricks'' of two principal sizes [28]. Above $\hbar \approx 2$ bricks are ''melted'' and chain properties become even more homogeneous along the chain. In the intermediate region irregular peaks come from different nonoverlapping instantons contributions, which as any tunneling effects are highly sensitive to small variations of potential barriers. Below their contributions are exponentially small, and above, as we see further, they overlap and form new *sliding* phase of the system.

In the following, we analyze in detail these regions, corresponding to different intervals of $\hbar$.

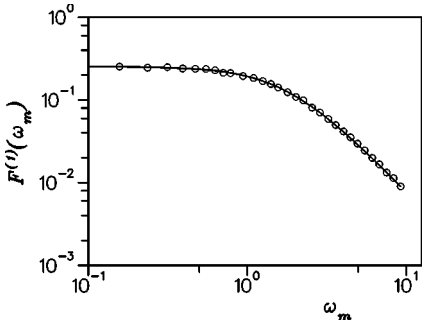


FIG. 2. The phonon spectral function $F^{(1)}(\omega_m)$ versus the rescaled frequency $\omega_m$, data are shown for the lowest spatial mode with $l=1$. The chain parameters are $s/r=89/55$, $K=5$, $\tau_0=80$, and $\hbar=0.8$. Here, $m$ varies from 1 to 89, but for clarity only selected values are shown. The solid curve gives the fit by Eqs. (16) and (17), open circles show numerical data. The fit determines the phonon frequency of the first mode ($\nu_1^2=3.170\pm0.012$) and the renormalization factor $f=1.0034\pm0.0034$.

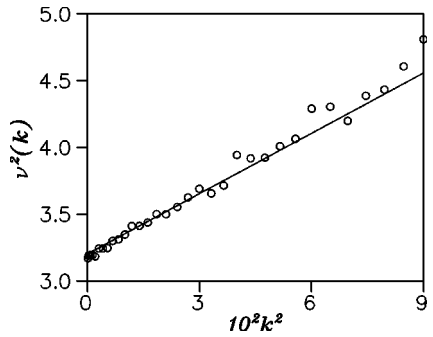


FIG. 3. The phonon dispersion law $\nu(k)$: open circles show the data obtained from the fit as it is shown in Fig. 2 for $l=1-30$ and the straight line shows the fit given by Eq. (20). The chain parameters are the same as in Fig. 2, the wave vector $k=\pi l/L$.

### B. Quasiclassical region $\hbar\lesssim1$

For $\hbar\lesssim1$ the tunneling between different metastable classical configurations is negligible, and the particles mainly vibrate around some classical equilibrium positions. In this case, the elementary excitations are phonons, and the quantization of the chain is reduced to the quantization of phonon modes, see, e.g., Ref. [18].

To single out low-energy excitations, we use the following approach. Of course, a particular excitation can be selected if the corresponding mode $V_j^{(l)}$ is known, but, in general, this is not a trivial task. However, for low-lying excitations one may expect that the modes have a simple harmonic form

$$V_j(k_l)\equiv V_j^{(l)}=\sqrt{\frac{2}{L}}\sin(k_l j),$$

$$k_l=\pi l/L \quad (l=1,2,\ldots), \tag{19}$$

where the wavelength $\lambda_l\equiv2\pi/k_l$ is much larger than a characteristic size of inhomogeneity in the chain. Direct numerical computations [31] of phonon modes in the classical FK chain support this ansatz (19).

The numerical test of this anzatz (19) is given in Fig. 2. Here, a typical result of the quantum simulations of the spectral function $F^{(l)}(\omega_m)$ is shown for the lowest phonon mode $l=1$ at $\hbar=0.8$. Fitting the data by Eq. (17) with the renormalization factor $f$ and the frequency of the phonon mode $\nu_l$ as free parameters, we obtain $f=1.0034\pm0.0034$ and $\nu_1^2=3.170\pm0.012$. This fit shows that the renormalization factor $f$ is remarkably close to unity, in spite of the fact that the value $\hbar=0.8$ is not small. Hence, ansatz (19) provides a good approximation to actual profiles of lowest phonon modes. This also indicates that the Gauss approximation used in the Sec. III A and in papers [16,19,20] works fine here. However, we note that at the same time the quantum effects renormalize substantially the phonon frequency ($\nu_1^2=3.170$) compared to its value at $\hbar=0.2$ ($\nu_1^2=3.706\pm0.019$). The computations for the classical FK chain give $\nu_1^2=3.717$ ($\hbar=0$).

These data show that at small $\hbar$ the frequency $\nu_1$ obtained from the quantum simulations approaches to the frequency of phonon mode in the classical chain. This fact gives a very important check of the consistency of our quantum simulations. We stress that a good agreement between the numerical data of Fig. 2 and the theoretical spectral function (17) takes place in the *whole* frequency range of $\omega_m$. This is, in fact, a very important consistency check of the good relaxation of our paths ensemble at all frequencies, including paths fluctuations at the lowest frequency available in the system.

By fitting the data for different phonon modes $l=1-30$ one can extract the dispersion relation for phonons $\nu(k)$, where $k=\pi l/L$ (see Fig. 3). The majority of data points follow the straight line given by the formula

$$\nu^2(k)=\nu_0^2+c^2k^2, \tag{20}$$

where $\nu_0$ is the phonon frequency gap and $c$ is the velocity of sound. The fit of numerical data gives $\nu_0^2=3.204\pm0.026$, $c^2=15.0\pm0.7$ for $\hbar=0.8$; $\nu_0^2=3.706\pm0.019$, $c^2=13.3\pm0.5$ for $\hbar=0.2$. These quantum data should be compared with the classical case where $\nu_0^2=3.697$, $c^2=11.5$ ($\hbar=0$). We note that there is a difference between the frequency of the first spatial harmonic $\nu_1$ and the frequency gap value $\nu_0$ obtained from the dispersion law. However, this difference is small and comparable with the statistical errors. For small $\hbar$ the parameters of the dispersion law converge to their classical values.

The described approach allows to obtain a complete information about low-energy phonon excitations in the whole quasiclassical region $\hbar\lesssim1$.

### C. Transition region $1\lesssim\hbar\lesssim2$

As it is seen from Fig. 1, this region corresponds to the transition between two regimes $\hbar\lesssim1$ and $\hbar\gtrsim2$, where the dependence of the quantum excitations on the particle location in the chain looks quite regular.

As it will be shown later the irregular behavior in the region $1 \lesssim \hbar \lesssim 2$ is related to a significant increase of the density of instantons. At high density the interaction between instantons becomes important and results in onset of new phonon branch at $\hbar > 2$. In this section, we discuss the properties of instantons and phonons and obtain estimates for their frequencies.

Let us start with a discussion of tunneling effects. For $\hbar < 1$ the contribution of tunneling to the spectral function is exponentially small being proportional to $\exp(-\text{const}/\hbar)$. However at $\hbar > 1$ the tunneling probability becomes large and it gives a significant contribution to the spectral function. The transition to this regime is seen in Fig. 1 as a sequence of sharp isolated peaks. Following the pioneering paper [32], a tunneling event can be associated to an *instanton*. In the imaginary time representation, the instanton is a local jump between two wells, which is fast compared to the mean time interval between subsequent jumps: while the size of instantons (in time $\tau$) is practically independent of $\hbar$, the separation between them is exponentially large in the quasiclassical limit (low instanton density). In particular, this means that in the first approximation one may consider instantons as independent jumps, as can be also checked from a direct examination of our path ensemble. Here, we should stress on two important properties of instantons in the quantum FK chain.

(i) Each jump of a particle $i$ in its position $x_i$ gives displacements of neighboring particles, which decay exponentially with the distance from the jump location, i.e., instantons are exponentially localized in space inside the chain.

(ii) Instantons are distributed inhomogeneously along the chain since the tunneling probability is highly sensitive to variations of barrier heights due to chain inhomogeneity.

A simple explanation of the exponential localization of an instanton (along the chain) comes from the fact that the new static configuration produced by it can be seen as a local *static* defect on the original configuration, which is known to die away exponentially with the classical Lyapunov exponent [6,23,24]. Indeed, in Fig. 1 one can see that at $\hbar \sim 1.2$–$1.3$ instanton contributions are exponentially peaked around some particular positions along the chain.

Let us now consider the properties of elementary excitations originated by instantons. There is a question how to select numerically a single instanton excitation. Obviously, ansatz (19) used for phonons is good only for extended modes, while instantons are localized in space. Therefore in this case, we analyze numerically the frequency spectrum of a given particle $i$ in the chain [defined by Eq. (11)]. If $\hbar$ is not too high (close to one), instantons do not overlap, and the main contribution to the spectrum comes from the instanton that is near to the given particle. This contribution reaches its maximum for a particle that actually jumps.

At the same time besides instanton jumps, the quantum motion of a particle in the chain contains a contribution of many phonons with different frequencies [see, e.g., Eq. (18)]. This phonon background should be subtracted in order to single out the contribution of instanton. Fortunately, the frequencies $\nu_l$ of phonon excitations are much higher than the frequency $\nu^{(inst)}$ of chosen instanton. Hence, these two types of excitations are well separated in the frequency domain.

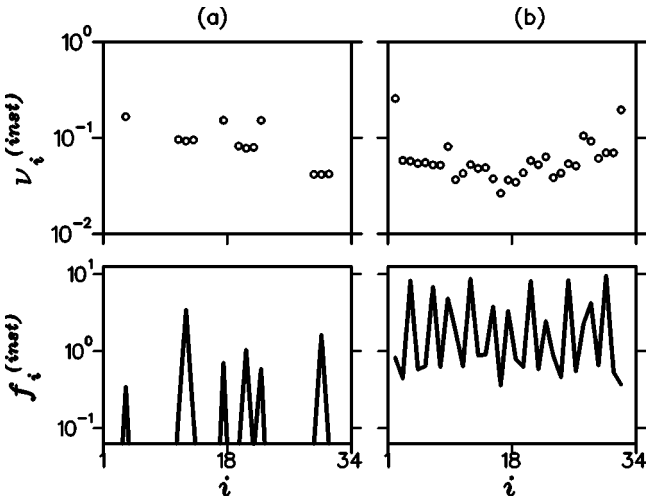


FIG. 4. Dependence of the instanton frequency $\nu_i^{(inst)}$ (top) and its weight $f_i^{(inst)}$ (bottom) on the position $i$ inside the chain (see text for explanations). (a) $\hbar = 1.2$ instantons do not overlap; the three highest peaks involves a group of three particles each. (b) $\hbar = 1.8$ instantons overlap. Chain parameters are $s/r = 34/21$, $K = 5$, and $\tau_0 = 320$.

Therefore, in our analysis of the instanton contribution to the spectral function $F_i(\omega_m) \equiv \langle |a_i(\omega_m)|^2 \rangle$, we can restrict ourselves to the frequency domain $\omega_m < \omega_{bound}$, where the boundary $\omega_{bound}$ is chosen by the condition $\nu^{(inst)} \ll \omega_{bound} \ll \nu_l$ for all phonon modes $l$. In this frequency domain, the phonon contribution (16) is practically independent of $\omega_m$ and can be replaced by some constant $C_i$. Thus, we can extract the frequency $\nu^{(inst)}$ and the weight $f_i^{(inst)}$ of the instanton excitation by following fit for the spectral function $F_i(\omega_m)$,

$$F_i(\omega_m) = f_i^{(inst)} \hbar / [\omega_m^2 + (\nu_i^{(inst)})^2] + C_i . \qquad (21)$$

This fit contains three free parameters $\nu_i^{(inst)}$, $f_i^{(inst)}$, and $C_i$.

If instantons do not overlap then one may expect that there are groups of particles whose motion is dominated by a single instanton. Inside each group, fit (21) should give the same values for the frequencies $\nu_i^{(inst)}$, while the variation of weight $f_i^{(inst)}$ with $i$ determines the instanton profile along the chain. This case is illustrated in Fig. 4(a), which corresponds to the early onset of instanton contribution at $\hbar = 1.2$. The six peaks in the bottom part of Fig. 4(a) show six nonoverlapping instantons, while the top part shows the corresponding frequencies as a function of particle index $i$ inside the chain. The peaks have different amplitudes, and the highest three of them involve groups of three particles that have the same frequency inside each group.

At higher $\hbar$ the number of instantons starts to grow rapidly and they begin to overlap. A direct confirmation of this trend is seen in Fig. 4(b) which corresponds to $\hbar = 1.8$. Here, all instantons have about 10% overlap with their neighbors and their interaction is rather strong. As a result the steplike structure of frequencies, seen at the top of Fig. 4(a), is practically destroyed. Thus, the instantons are ''collectivized''

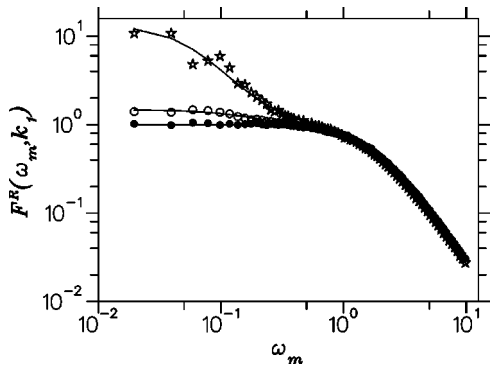


FIG. 5. Rescaled spectral function $F^R(\omega,k_1)=(\nu_1^2/\hbar)F(\omega,k_1)$ at the very beginning of instanton onset. The bump which appears at $\omega\lesssim 0.2$ corresponds to instanton admixture to the phonon spectral function. Black points, open circles, and stars correspond to $\hbar=1$, 1.1, and 1.2. Lines show the fit to numerical data with Eq. (22). Chain parameters used in simulations are $s/r=34/21$, $K=5$, and $\tau_0=320$.

and the consideration of a single instanton as one-particle jump over barrier becomes not adequate. At higher $\hbar$ values, this process leads to appearance of a new phonon mode.

Let us now discuss the phonon properties in the region $1\lesssim\hbar\lesssim 2$. As in Sec. III B, we extract them from the spectral function $F(\omega_m,k_l)\equiv F^{(l)}(\omega_m)$ obtained on the basis of ansatz (19) for a phonon mode $l$. However, in this region of $\hbar$ the spectral function $F^{(l)}(\omega_m)$ has an admixture of instantons, which grows rapidly with $\hbar$; a change of $\hbar$ from 1.1 to 1.2 results in more than ten times of the admixture weight (see Fig. 5). We note that in the absence of instanton contribution the rescaled phonon spectral function $F^R(\omega,k_l)\equiv(\nu_l^2/\hbar)F(\omega,k_l)$ plotted in Fig. 5 should have an universal limit equal to unity independent of the value of $\hbar$. Hence, the increase of $F^R(\omega,k_l)$ at small $\omega$ stresses the important contribution of instantons. These instantons have different frequencies and their contribution to the spectral function can be rather complicated. However, we can use again the strong frequency separation between instanon and phonon excitations. Indeed, for $\omega_m\gtrsim\nu_l\gg\nu^{(inst)}$, all instanton contributions have an universal behavior $\propto\omega_m^{-2}$. Therefore, we may replace them by a single ''instanton contribution'' with some average instanton frequency $\overline{\nu^{inst}}$. Then, the spectral function can be fitted by a sum of two contributions

$$F(\omega_m,k_l)=f_{ph}\hbar/[\omega_m^2+\nu_l^2(k_l)]+f_{inst}\hbar/\{\omega_m^2+[\overline{\nu^{inst}}(k_l)^2]\}, \tag{22}$$

where $f_{ph}(k),\nu_l(k)$, and $f_{inst}(k),\overline{\nu^{in}}(k)$ are free fit parameters for phonons and instantons, respectively.

Fitting the data for different phonon modes at $l=1-30$, we extract the phonon dispersion law (20) (see Fig. 6, compare with fit procedure for $\hbar<1$). Contrary to the case of Fig. 3 at $\hbar<1$, now the data for the dispersion law $\nu(k)$ are scattered inside some finite band. This indicates that anzatz (19) for the phonon profile is not so good to single out particular phonon modes. Actually, the width of the band provides some measure of the inaccuracy. Nevertheless, the phonon modes are still approximately defined in the domain of $\hbar$ under consideration. Their frequency decreases as $\hbar\to 2$ but remains separated from zero by a finite gap.

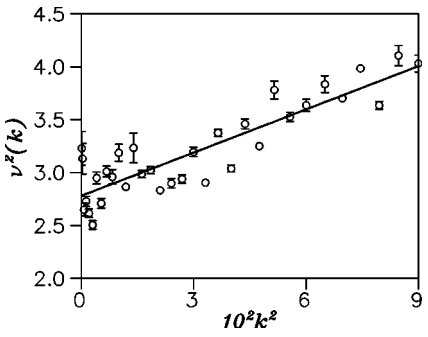


FIG. 6. Frequency $\nu(k)$ of phonons versus wave number $k$ obtained from fit (22) at $\hbar=1.5$ (in the middle of the transition region). Chain parameters used in simulations are $s/r=89/55$, $K=5$, and $\tau_0=80$.

We also note that fit (22) allows formally to determine the dispersion law $\nu_{inst}(k)$ for the instanton branch. However, the numerical data give irregular scattering of points inside a band $0\leqslant\nu_{inst}^2\lesssim 0.01$ without any clear dependence on $k$. The reason of such behavior is simple; projections of irregular positions of instantons on the harmonic ansatz (19) produce random weights for contributions of different instantons. This result represents another manifestation of glasslike structure formed by instantons frozen or pinned inside the chain. Since the positions of instantons are random the phonons cannot propagate along the chain on large distances. In fact, they become localized by disorder in a way similar to the one-dimensional Anderson localization (more details on the phonon properties in this regime will be presented elsewhere [31]).

### D. New sliding phonon branch at $\hbar>2$

From Fig. 1 one can see that the variation of the amplitude $a_i(\omega_1)$ with $i$ (low-frequency excitations) becomes

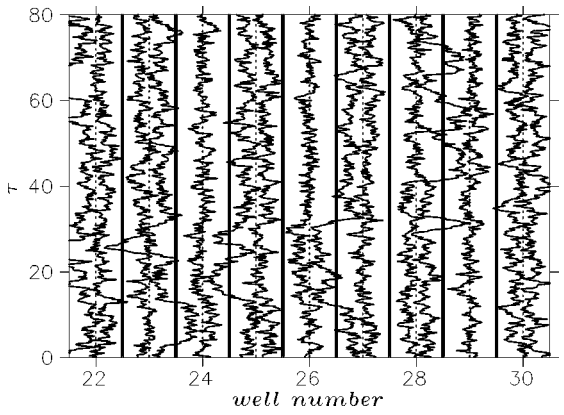


FIG. 7. A sample of quantum paths of particles inside some chain fragment, which corresponds to periods of the external potential with numbers 22–30. Dashed lines show bottoms of the wells, thick solid lines show the tops of the barriers. Note an example of highly correlated instanton transitions at $\tau=15-30$ which involve particles in up to five periods of the potential. Parameters of the simulation are $\hbar=2.3$, $s/r=89/55$, $K=5$, and $\tau_0=80$.

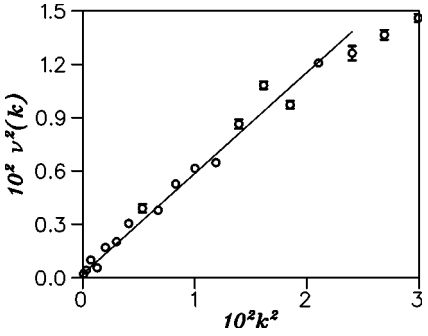


FIG. 8. The dispersion law $\nu(k)$ for sliding phonons at $\hbar=2.5$. The numerical data (circles with error bars) are obtained from fit (22) for the instanton branch $\nu_{inst}(k_l)$. The straight line shows the best fit (20) to numerical data. The chain parameters used in simulations are $s/r=89/55$, $K=5$, and $\tau_0=80$.

rather smooth at $\hbar>2$. This means that the instantons are strongly overlapped here. In fact, this means that several particles of some chain fragment jumps from one well to the next simultaneously (see Fig. 7). This is nothing but sliding of a local chain fragment along the periodical potential. The typical size of such fragments should grow with $\hbar$. If their sizes reach the size of the chain then the sliding mode becomes open, and the phonon gap disappears. At this point the pinned instanton glass turns into the sliding phonon gas.

A confirmation of this picture is presented in Fig. 8, which corresponds to $\hbar=2.5$ being just above the transition point $\hbar_c\approx 2$. The numerical data for the dispersion law $\nu(k)$ in Fig. 8 are obtained from fit (22) at $\hbar>2$. Here, the behavior of phonon and instanton modes changes dramatically: phonons data $\nu(k)$ are now irregularly scattered over a wide band, while the data points for instanton branch follow a single line, reproducing fairly well a phononlike dispersion law with zero gap (see Figs. 8 and 9). In particular, fit (20) gives $\nu_0=0.04\pm 0.01$, which is close to zero. In fact, this value is smaller than the minimal frequency $2\pi/\tau_0$ ($\approx 0.079$, at $\tau_0=80$) and therefore it is compatible with zero.

On the contrary, the wide scattering of data points for the phonon branch indicates that ansatz (19) is not good for phonon contribution at $\hbar\gtrsim 2$ (see Fig. 9). This scattering of points is related to the localization of high-frequency phonon modes. In contrast, a smooth behavior of data points for the instanton branch demonstrates that the instanton wave functions become close to the harmonic wave ansatz (19). Hence, these excitations are delocalized. This leads us to the conclusion that for $\hbar>2$ the instanton branch is replaced by a new gapless branch of new sliding phonons.

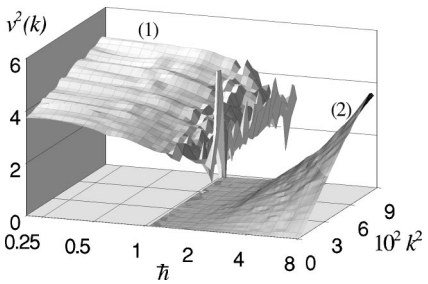


FIG. 9. The frequency $\nu(k)$ of elementary excitations versus the wave number $k$ at different $\hbar$. Chain parameters used in simulations are $s/r=89/55$, $K=5$, and $\tau_0=80$. The two sheets 1 and 2 refer to phonon and instanton excitations, respectively.

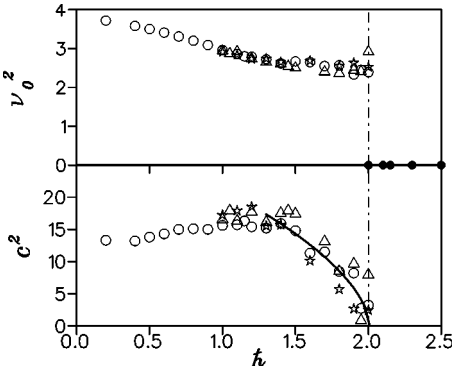


FIG. 10. Dependence of the phonon gap $\nu_0$ and sound velocity $c$ on $\hbar$ for the case of Fig. 9 at $K=5$. Open symbols correspond to sheet 1 in Fig. 9. Circles and triangles are obtained at $\tau_0=80$ for chain sizes $s/r=89/55$ and 233/144, respectively. Stars correspond to $s/r=34/21$ and $\tau_0=320$. The solid line (bottom) gives fit (23) for $1.3\leqslant\hbar\leqslant 2$ (see text). The full circles (top) for $\hbar>2$ refer to the sliding phonon branch from sheet 2 of Fig. 9, they indicate a zero phonon gap.

### E. Global picture of elementary excitations in the FK chain

The ensemble of data for the dispersion law $\nu(k)$ of elementary excitations at different values of $\hbar$ is shown in Fig. 9 by the two sheets representing the phonon branch (1) and the instanton branch (2). The numerical data are obtained with ansatz (19) by fit (22).

Sheet 1 refers to phonons originated from classical phonon modes, which are well reproduced in the limit $\hbar\to 0$. The frequencies of these modes are well separated from zero by a large gap. Therefore, one may say that they form the optical phonon branch. At $\hbar\gtrsim 1$ these modes show a tendency to become softer and at $\hbar\gtrsim 1.5$ their dependence on $k$ and $\hbar$ becomes irregular. As it was explained in the preceding section, this irregular dependence is related to the glasslike structure of randomly pinned instantons where density increases with the growth of $\hbar$. Sheet 2 appears at $\hbar<2$ from the instanton contributions into the Feynman path integral. For $\hbar>\hbar_c\approx 2$ this instanton branch turns into a new gapless branch of sliding phonons (see the discussion related to Fig. 8).

A more quantitative picture can be obtained from the numerical data for the gap $\nu_0$ and the sound velocity $c$ for both sheets in Fig. 9. For the optical phonon branch the values of $\nu_0$ and $c$ are determined from fit (22) for different values of $\hbar$ (see Fig. 10). The data show that the phonon gap remains finite and large at $\hbar<\hbar_c\approx 2$. In contrast, the sound velocity $c$ drops to zero as $\hbar$ approaches the value $\hbar_c$. This decay is compatible with the fit

$$c^2=a(\hbar_c-\hbar)^\alpha, \tag{23}$$

shown by the solid line with $a=20.5\pm 1.3$, $\hbar_c=2.0\pm 0.1$, and the critical exponent $\alpha=0.52\pm 0.07$. Even if the numeri-

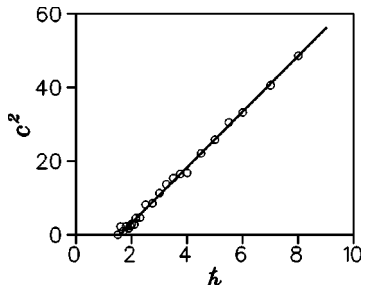


FIG. 11. Dependence of sound velocity $c$ on $\hbar$ for excitations on the soft phonon sheet 2 in Fig. 9. Points correspond to chain parameters $s/r=89/55$, $K=5$, and $\tau_0=80$. The solid line shows the linear fit to the sound velocity data inside the region $\hbar>2$ (see text).

cal data for $c$ have certain fluctuations they still clearly indicate the quantum phase transition at $\hbar_c\approx 2$, where the sound velocity $c$ drops to zero. Further extensive numerical studies are required to determine the behavior in the vicinity of transition in a more precise way.

For the sliding phonon branch, we extract the parameters $\nu_0$ and $c$ from the data of sheet 2 in Fig. 9 using a more general fit given by

$$\nu^2(k)=\nu_0^2+c^2k^2/(1+k^2/k_B^2).$$

Compared to the standard case (20), we introduce an additional parameter $k_B$ to take into account the saturation of $\nu(k)$ at large $k$ (see, Figs. 8 and 9). The numerical data show that the gap $\nu_0$ is small and does not exceed the minimal frequency in the system $\varpi=2\pi/\tau_0$. Hence, the gap $\nu_0$ is compatible with zero [see Fig. 10 (top)]. At the same time the sound velocity $c$ for the sliding phonon branch grows approximately linearly with $\hbar$ (see Fig. 11). The best fit of numerical data for $\hbar>2$ gives

$$c^2=a(\hbar-b), \tag{24}$$

with $a=7.6\pm 0.1$, $b=1.57\pm 0.05$. Formally, the value of $b$ is different from the value $\hbar_c=2.0$ in Eq. (23). However, in view of large statistical fluctuations both fits for optical phonons and sliding phonons are compatible with the quantum phase transition at $\hbar_c\approx 2$. Indeed, the formal statistical error given by the error bars do not take into account a possibility that in the vicinity of critical point the sound velocity may have systematic deviations from the simple fit used in Eq. (24). Also it is well known that the formal power law fits are not very accurate in the vicinity of a critical point. From this point of view a slight difference for the critical values of $\hbar_c$ are acceptable. In addition, the longwave response gives $\hbar_c\approx 2$ (see Sec. IV B).

### F. Time correlations

Time correlations are closely related to the frequency spectrum of elementary excitations in the system. Their analysis is probably the most traditional way to extract properties of the elementary excitations, see, e.g., Refs. [33,34]. Below, we discuss the connection of this traditional method with our approach based on the Fourier spectrum of Feynman paths described above. We compare the results obtained by these two different methods.

The one-particle time correlators are directly related to the Fourier spectrum of Feynman paths, and are given by the following expression:

$$\langle x_i(0)x_i(\tau)\rangle=\frac{1}{\sqrt{\tau_0}}\sum_{\omega_m}|a_i(\omega_m)|^2\exp(-i\omega_m\tau).$$

In fact, many elementary excitations with different frequencies contribute to a particle motion in the chain. In order to single out a particular phonon mode, we study the correlators of normal modes $X^l(\tau)=\Sigma_i V_i^{(l)}x_i(\tau)$ where $V_i^{(l)}$ are eigenvectors defined in Eqs. (13) and (14). Then from Eq. (15), we obtain

$$\begin{aligned}\langle X^l(0)X^l(\tau)\rangle&=\frac{1}{\sqrt{\tau_0}}\sum_{\omega_m}|A^l(\omega_m)|^2\exp(-i\omega_m\tau)\\&=\langle(X^l(0))^2\rangle(e^{-\nu_l\tau}+e^{-\nu_l(\tau_0-\tau)}),\end{aligned}\tag{25}$$

where $\langle(X^l(0))^2\rangle=\hbar/2\nu_l$ is the contribution of a single phonon mode and the periodicity along the time torus results in a second exponential term in Eq. (25).

However, Eq. (15) assumes only small quantum fluctuations ($\sim\hbar$) around some *classical* trajectory. But due to the tunneling effects (or instantons) a particle jumps from one *classical* trajectory to another and its actual motion is given by a sum of phonon $x_i^{(ph)}(\tau)$ and instanton $x_i^{(inst)}(\tau)$ contributions:

$$x_i(\tau)=x_i^{(ph)}(\tau)+x_i^{(inst)}(\tau).$$

In general, both motions influence each other, but in the quasiclassical limit $\hbar\to 0$ they can be considered as independent. In this limit, they have quite different frequency scales; the phonon frequency $\nu_l$ is of the order of $K^{1/2}$, while the frequency of tunneling jumps $\nu_{inst}$ is exponentially small. In contrast, while the amplitude of phonon oscillations in the limit $\hbar\to 0$ is small: $\langle[x_i^{(ph)}(\tau)]^2\rangle\propto\hbar$, the amplitude of jumps is defined by the difference between equilibrium particle positions in two neighboring wells (in our case it is $\sim 3$–$4$), i.e., it does not depend on $\hbar$. Hence, for a jumping particle $\langle[x_i^{(inst)}(\tau)]^2\rangle\sim 10$ which is not small even in the quasiclassical limit $\hbar\to 0$. Therefore, the instanton contribution to the time correlator has the form [34]

$$\langle x_i(0)x_i(\tau)\rangle_{inst}=\langle[x_i^{(inst)}(\tau)]^2\rangle(e^{-\nu_{inst}\tau}+e^{-\nu_{inst}(\tau_0-\tau)}).\tag{26}$$

The preexponent factor is large for jumping particles even in the deep quasiclassical regime.

In fact, not any particle can easily jump from one well to another: different classical trajectories have different actions and all jumps that result in a large change of action $\Delta S\gtrsim\hbar$ are inhibited. In particular, it is clearly seen in Fig. 1 that the number of instanton peaks is smaller at smaller $\hbar$ since the contribution of transitions with large difference in action $\Delta S$ is suppressed.

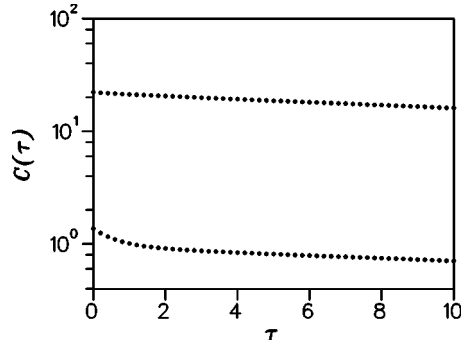


FIG. 12. The numerically computed time correlator $C(\tau)=\langle X^l(0)X^l(\tau)\rangle$ for $l=1$ at different time separations $\tau$ for $\hbar=1.4$ (lower points) and $\hbar=2.5$ (upper points). The parameters of the chain are $s/r=89/55$, $K=5$, and $\tau_0=80$.

Finally, the general form for the time correlator that takes into account the instantons contribution takes the form

$$C(\tau)\equiv\langle X^l(0)X^l(\tau)\rangle=\langle (X^l(0))^2\rangle(e^{-\nu_l\tau}+e^{-\nu_l(\tau_0-\tau)})$$

$$+\sum_{inst} w_{in}(e^{-\nu_{inst}\tau}+e^{-\nu_{inst}(\tau_0-\tau)}). \qquad (27)$$

Here, the first term describes the phonon contribution and in the second term the sum is taken over instantons and the instanton weights $w_{inst}=\Sigma_{i,k}V_i^{(l)}V_k^{(l)}\langle x_i(0)x_k(0)\rangle$ describe the overlap with ansatz (19). Both types of contributions (27) are clearly seen in Fig. 12 at $\hbar=1.4$. The initial rapid drop at $\tau\lesssim 1.5$ corresponds to phonon contribution, while the slow decay at $\tau>1.5$ corresponds to the instanton contribution. This initial drop is related to the existence of large quasiclassical gap for phonon excitations. For $\hbar=2.5>\hbar_c$, the gap disappears and the correlator decay very slowly (see Fig. 12).

For $\hbar>\hbar_c$, we have a new phase where instantons are replaced by sliding phonons. Therefore in this regime, we fit the numerical data for $C(\tau)$ by Eq. (27) with $w_{inst}=0$. The results for different $l$ allow to obtain numerically the dispersion law $\nu(k)$ shown in Fig. 13 (open circles). However, the accuracy of this data is not so good compared to data (full circles) obtained from the analysis of Fourier spectrum of Feynman paths described in the previous sections.

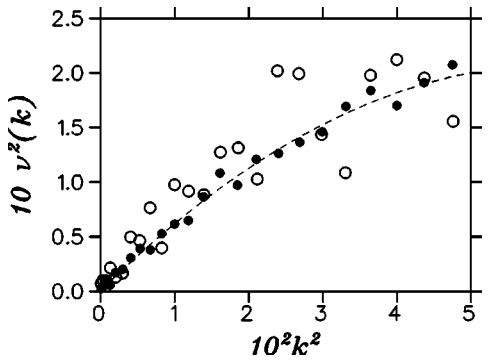


FIG. 13. Frequency of elementary excitations $\nu(k)$ versus $k$ for sliding phonon branch at $\hbar=2.5$. Open circles show data extracted from the time correlator $C(\tau)$ for different $l$ (see Fig. 12), full circles present the results obtained from fit (22) for the frequency spectrum of Feynman paths (see Fig. 8). The chain parameters are the same as in Fig. 12.

## IV. QUANTUM PHASE TRANSITION

The structual rearrangement of the elementary excitations spectrum can be related to the *quantum phase transition* in the chain from a pinned to sliding phase. However, we would like to stress that in contrast to the classical picture [23,24] in the quantum case the absence of energy gap for excitations is not necessarily related to the opening of the sliding phase. Indeed, due to quantum tunneling through Peierls-Nabbarro barriers related to instantons there are excitations with energy which decreases exponentially with the increase of barrier heights. Formally, this corresponds to the disappearance of excitation gap. Therefore, to confirm firmly the appearance of sliding phase, we need to consider spatial correlations of particle motion in the chain. The sliding phase appears when the spatial correlation length becomes comparable with the length of the chain.

### A. Spatial correlation length

The analysis of spatial correlations (correlations between the motion of different particles in the chain) is the most evident way to observe the transition between pinned and sliding phases. In principle, the spatial correlation function can be explicitly computed if the spectrum and the wave functions of elementary excitations are known. In fact, we have a complete quantitative picture for *phonon* modes, at least for the low-lying ones. To obtain numerically the value of the spatial correlation length $l_c$, we assume that the elementary excitation spectrum is given by the dispersion relation $\nu^2(k)=\nu_0^2+c^2k^2$ and the corresponding phonon modes are given in ansatz (19). Then the same-time spatial correlator reads

$$\langle (x_i-\langle x_i\rangle)(x_j-\langle x_j\rangle)\rangle=\sum_l V_i^{(l)}V_k^{(l)}\langle [X^l(0)]^2\rangle$$

$$=\hbar\sum_k \frac{\cos[k(i-j)]}{L\nu(k)}$$

$$=\frac{\hbar}{\pi c}K_0(|i-j|/l_c), \qquad (28)$$

where $K_0(x)$ is McDonald's function, with a known asymptotics: $K_0(x)\to_{x\to\infty}\sqrt{(\pi/2x)}e^{-x}$ and $l_c=c/\nu_0$.

Fit (28) of the numerical data gives the value of $l_c$ for different values of $\hbar$ as it is shown in Fig. 14. It is seen that the length $l_c$ has a sharp increase at $\hbar_c\approx 2$, and for $\hbar>\hbar_c$ it becomes comparable with the length of the chain. This indicates that we have the *quantum phase transition* near $\hbar_c\approx 2$. Indeed at $\hbar<2$ the length $l_c$ is practically independent of the chain length $L$, while at $\hbar>2$ it starts to increase with $L$. This is confirmed by the data of Fig. 14, where in spite of strong fluctuations for $\hbar>2$ the length $l_c$ becomes comparable with the chain size $L$.

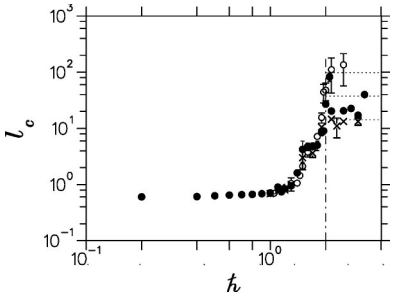


FIG. 14. The dependence of the spatial correlation length $l_c$ on $\hbar$. Crosses, full, and open circles correspond to chains with $s/r=34/21$, 89/55, and 233/144, respectively; $K=5$, $\tau_0=80$. The vertical dot-dashed line marks the quantum phase transition at $\hbar_c \approx 2$. The positions of the horizontal dotted lines are proportional to the chain length $L=2\pi r$.

### B. Longwave response

The appearance of the new sliding phonon phase implies that the response of amplitude of the longwave modes should be large in this regime. To test this expectation, we present the dependence of the amplitude $A^l(\omega=0)$ on $\hbar$ in Fig. 15. The numerical data demonstrate a sharp increase of $A^l(0)$ near $\hbar_c \approx 2$. It is interesting to note that due to the existence of frequency gap for phonon excitations at $\hbar<\hbar_c$ the amplitude $A^l(0)$ is not very sensitive to the variations of $l$. On the contrary, for $\hbar>\hbar_c$ the gap disappears and $A^l(0)$ starts to depend on $l$ [see Fig. 15(a)]. In a similar way $A^l(0)$ is independent of the chain length $L$ for $\hbar<\hbar_c$, while at $\hbar>\hbar_c$ it grows with $L$ [see Fig. 15(b)]. The numerical data of Fig. 15(b) for $1.5\leqslant\hbar\leqslant 2$ can be described by the fit

$$\langle [A^l(0)]^2\rangle \approx A(\hbar_c-\hbar)^{-\gamma}, \tag{29}$$

which gives $\gamma=5.06\pm1.72$ and $\hbar_c=2.01\pm0.05$.

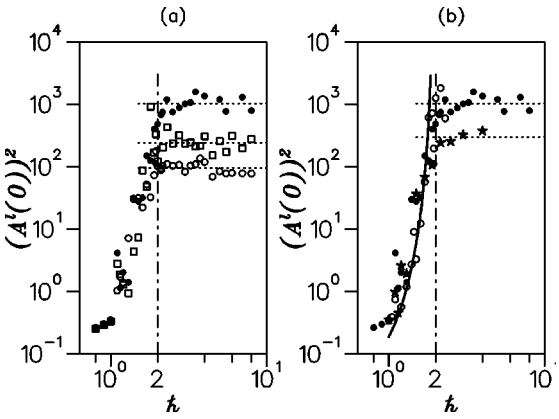


FIG. 15. The amplitude square of zero-frequency quantum fluctuations $[A^l(0)]^2$ as a function of $\hbar$ for $K=5$ and $\tau_0=80$. (a) Full circles, squares, and open circles are for modes $l=1,3$, and 5, respectively, for the chain with $s/r=89/55$. (b) Open circles, full circles, and stars are for $s/r=233/144$, 89/55, and 34/21, respectively; $l=1$. The vertical dot-dashed lines mark $\hbar_c \approx 2$, the horizontal dotted lines give the average values for $\hbar>2$.

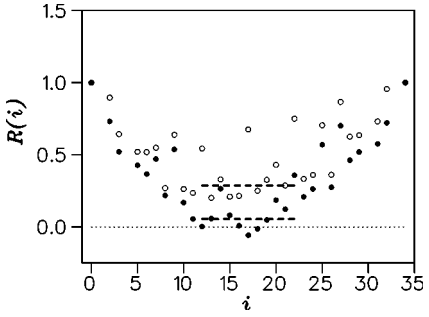


FIG. 16. Dependence of the response function $R(i)$ on the particle position $i$ in the chain at $\hbar=1.8$ (full circles) and $\hbar=2.2$ (open circles). The horizontal dashed lines show the interval of averaging for the minimal response value $R_{min}$ in Fig. 17. Parameters of the chain are $s/r=34/21$, $K=5$, and $\tau_0=80$.

### C. Other characteristics

Another way to test the transition from the pinned instanton glass to the sliding phonon phase is to measure the sensitivity to small shifts of boundaries of the chain. With this aim, we consider the shift of boundary particles $i=0$ and $i=s$ given by

$$x_0(\tau)=a_S\cos(2\pi\tau/\tau_0), \quad x_s(\tau)=x_0+L, \tag{30}$$

where the amplitude $a_S$ was fixed at $a_S=0.5$. In Fig. 16, we present the dependence of the response function $R(i)=\langle x_0(x_i-\langle x_i\rangle)\rangle/\langle x_0^2\rangle$ on the particle number $i$ inside the chain. It is seen that the response in the center of the chain drops strongly when the parameter $\hbar$ changes from $\hbar=2.2$ to $\hbar=1.8$. This means that the chain is locked for $\hbar<\hbar_c\approx 2$, while for $\hbar>\hbar_c$ the chain slides following the displacements of the boundary particles.

In order to get a more quantitative picture, we estimate the value of the response function $R(i)$ at its minimum in the middle of the chain by taking its average value inside the central region at $i=12$–22: $R_{min}=\langle R(i)\rangle_i$ (this interval is shown in Fig. 16 by horizontal dashed lines). The dependence of $R_{min}$ on the parameter $\hbar$ is presented in Fig. 17. We see that the correlator in the central region of the chain deviates from zero at $\hbar>2$. According to the numerical data the response $R_{min}$ is very small for $\hbar<\hbar_c\approx 2$, while it becomes rather strong for $\hbar>\hbar_c$. This confirms the existence of the quantum phase transition from the pinned to sliding phase at $\hbar=\hbar_c\approx 2$.

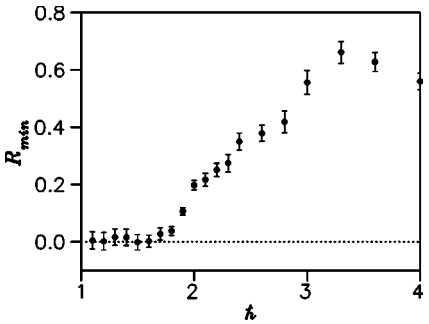


FIG. 17. Dependence of the minimal response $R_{min}$ on $\hbar$ for the parameters of Fig. 16.

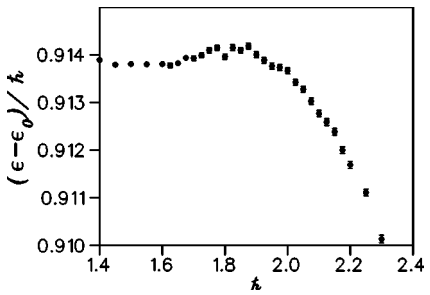


FIG. 18. Dependence of the total chain energy per particle on $\hbar$ for the chain parameters $K=5$, $s/r=89/55$, and $\tau_0=80$; $\epsilon_0=5.302$ is an energy point chosen from convenience or illustration reasons.

What is the order of this transition? In our simulations, we have repeated a cycle changing slowly $\hbar$ from $\hbar=1$ to $\hbar=4$ and back about hundred times, but no hysteresis was found within the statistical errors. Indeed, the difference of the chain energy per particle at the upward and backward paths did not exceed $10^{-3}$. This difference should be compared with the change of the energy per particle $\delta E\approx 2.4$ which takes place when $\hbar$ changes from $\hbar=1$ to $\hbar=4$. The absence of hysteresis excludes the phase transition of the first order. We also do not see any breaks in the dependence of the chain energy on $\hbar$. In order to make small deviations from a linear law more visible, we plot in Fig. 18 the quantity $(\epsilon-\epsilon_0)/\hbar$, where $\epsilon_0=5.302$. The numerical data show that the slope of energy dependence changes near $\hbar=\hbar_c\approx 2$. This change of slope is located approximately at the same value of $\hbar$ where the divergence of the correlation length takes place (see Fig. 14). These data indicate that we have a second-order quantum phase transition that appears near $\hbar_c\approx 2$. However, more extensive numerical simulations are required to determine more precisely the order of the transition.

## V. CONCLUSIONS

We have studied quantum tunneling phenomena in a particular model of glassy material, the Frenkel-Kontorova chain. This system has a lot of states, which are exponentially degenerate and (meta)stable in the (quasi)classical limit. In the quantum case, there are tunneling transitions between these states that can be understood in terms of instanton dynamics. In the quasiclassical limit, at small $\hbar$ the instanton density is small and instantons are local and isolated. With the increase of $\hbar$ their density grows and they start to overlap.

At sufficiently large $\hbar$ the instantons are coupled and become collectivized. As a result, the tunneling of particles in some fragments of the chain proceeds in correlated way. The size of these correlations grows until it reaches the size of the system. This leads to appearance of extended excitations and opening of a new gapless sliding phonon branch. Our data show that a quantum phase transition takes place between the pinned and sliding phases. Absence of hysteresis effects, as well as continuous dependence of chain energy on $\hbar$ exclude the first-order phase transition, so we can classify this transition as a continuous quantum phase transition. We stress that the quantum phase transition from pinned to sliding phase takes place in the regime where the classical chain always remains in the pinned phase with the finite phonon gap.

The direct analysis of Fourier spectrum of Feynman paths ensemble allowed to obtain detailed information on the dispersion law of low-lying excitations in both quantum phases. Nevertheless, some questions remain open for further investigations. For example, one can analyze in more detail the effects of interactions between instantons at low density and study their propagation properties in this regime. Another interesting remark concerns the behavior of the system in the vicinity of the transition point at $\hbar_c\approx 2$. Indeed, in this region the kinetic energy per particle is $\approx 0.6$, that is, about ten times smaller than the height of the potential barrier at $K=5$. Therefore, more insights are required to understand the underlying physics of this transition.

One can ask on how general are our results obtained in the frame of the Frenkel-Kontorova model? In fact, we never used any specific features of this model related to its nontrivial number theory properties. The only essential point is the existence of an exponential number of quasidegenerate states which is common for glassy materials and other disorder systems. Therefore, it is very interesting to study an analogous quantum phase transition in systems with disorder and interactions.

## ACKNOWLEDGMENTS

This work was supported in part by the EC RTN network Contract No. HPRN–CT-2000-0156; O.V.Z. thanks the groups in Como and Toulouse for their hospitality during the work on this problem.

[1] Y.I. Frenkel and T.K. Kontorova, Zh. Éksp. Teor. Fiz. **8**, 1340 (1938) [Phys. Z. Sowjetunion **13**, 1 (1938)].
[2] F. Nabarro, *Theory of Crystal Dislocations* (Clarendon, Oxford, 1967).
[3] V.L. Pokrovsky and A.L. Talapov, *Theory of Incommensurate Crystals*, Soviet Scientifical Reviews Supplement Series Physics Vol. 1 (Harwood, London, 1984).
[4] S.C. Ying, Phys. Rev. B **3**, 4160 (1971).
[5] L. Pietronero, W.R. Schneider, and S. Strässler, Phys. Rev. B **24**, 2187 (1981).
[6] S. Aubry, in *Solitons and Condensed Matter Physics*, edited by A.R. Bishop and T. Schneider (Springer, New York, 1978).
[7] S. Aubry, J. Phys. (France) **44**, 147 (1983).
[8] L.M. Floria and J.J. Mazo, Adv. Phys. **45**, 505 (1996).
[9] O.M. Braun, T. Dauxois, M.V. Paliy, and M. Peyrard, Phys. Rev. Lett. **78**, 1295 (1997); Phys. Rev. E **55**, 3598 (1997).
[10] L. Consoli, H.J.F. Knops, and A. Fasolino, Phys. Rev. Lett. **85**, 302 (2000).
[11] F. Borgonovi, I. Guarneri, and D. Shepelyansky, Phys. Rev. Lett. **63**, 2010 (1989).

[12] F. Borgonovi, I. Guarneri, and D. Shepelyansky, Z. Phys. B: Condens. Matter **79**, 133 (1990).
[13] F. Borgonovi, Ph.D. thesis, Universita degli Studi di Pavia, Italia, 1989.
[14] G.P. Berman, E.N. Bulgakov, and D.K. Campbell, Phys. Rev. B **49**, 8212 (1994).
[15] G.P. Berman, E.N. Bulgakov, and D.K. Campbell, Physica D **107**, 161 (1997).
[16] B. Hu, B. Li, and W.M. Zhang, Phys. Rev. E **58**, R4068 (1998).
[17] B. Hu and B. Li, Europhys. Lett. **46**, 655 (1999).
[18] B. Hu, B. Li, and H. Zhao, Europhys. Lett. **53**, 342 (2001).
[19] B. Hu and B. Li, Physica A **288**, 81 (2000).
[20] C.-L. Ho and C.-I Chou, Phys. Rev. E **63**, 016203 (2001).
[21] B.V. Chirikov, Phys. Rep. **52**, 263 (1979).
[22] I.C. Percival, in *Nonlinear Dynamics and the Beam-Beam Interaction*, edited by Melvin Month and John C. Herra, AIP Conf. Proc., No. 57 (AIP, New York, 1979), p. 302.
[23] S. Aubry, Physica D **7**, 240 (1983).
[24] S. Aubry and P.Y. Le Daeron, Physica D **8**, 381 (1983).
[25] R.S. MacKay, J.D. Meiss, and I.C. Percival, Physica D **13**, 55 (1984).
[26] R. Schilling, Phys. Rev. Lett. **53**, 2258 (1984).
[27] P. Reichert and R. Schilling, Phys. Rev. B **32**, 5731 (1985).
[28] O.V. Zhirov, G. Casati, and D.L. Shepelyansky, Phys. Rev. E **65**, 026220 (2002).
[29] T. Shaefer and E.V. Shuryak, Rev. Mod. Phys. **70**, 323 (1998).
[30] H.U. Beyeler, L. Pietronero, and S. Strässler, Phys. Rev. B **22**, 2988 (1980).
[31] O.V. Zhirov, G. Casati, and D.L. Shepelyansky (unpublished).
[32] A. Polyakov, Nucl. Phys. B **120**, 429 (1977).
[33] M. Creutz and B. Freedman, Ann. Phys. (N.Y.) **132**, 427 (1981).
[34] E.V. Shuryak and O.V. Zhirov, Nucl. Phys. B **242**, 393 (1984).
[35] S.L. Sondhi, S.M. Girvin, J.P. Carini, and D. Shahar, Rev. Mod. Phys. **69**, 315 (1997).
[36] N. Metropolis, A. Rosenbluth, M. Rosenbluth, A. Teller, and E. Teller, J. Chem. Phys. **21**, 1087 (1953).